Eur. Phys. J. Plus (2022) 137:1180
https://doi.org/10.1140/epjp/s13360-022-03378-z

THE EUROPEAN PHYSICAL JOURNAL PLUS

Regular Article

Excitation functions of deuteron induced nuclear reactions on dysprosium targets for the production of the theranostic relevant isotopes of terbium

Michele Colucci[1,2,a], **Stefano Carminati**[1,2,b], **Ferid Haddad**[3,4,c], **Etienne Nigron**[4,d], **Flavia Groppi**[1,2,e], **Simone Manenti**[1,2,f]

[1] Department of Physics, University of Milan, via Celoria 16, I-20133 Milan, Italy
[2] LASA, University of Milan and INFN-Milano, via F.lli Cervi 201, I-20090 Segrate, MI, Italy
[3] Laboratoire Subatech, IN2P3-CNRS, IMT Atlantique, Nantes Université, 4 rue Alfred Kastler, 44307 Nantes, France
[4] GIP Arronax, 1 rue Aronnax, 44817 Saint-Herblain, France

Received: 18 August 2022 / Accepted: 9 October 2022

Abstract The physical properties of ^{149,152,155,161}Tb enable their use in both diagnostic and therapeutic applications in the field of nuclear medicine. For this reason the optimization of the production routes of these radionuclides is of widespread interest in research. In this work, the feasibility of the production of ^{155}Tb and ^{161}Tb via the nuclear reactions induced by deuterons on dysprosium target with natural isotopic abundances has been discussed. The cross sections of ^{nat}Dy(d,x) reactions have been studied in the 12.5–32 MeV energetic range with the stacked-foil technique and the corresponding Thick Target Yields have been obtained. The presence of terbium and dysprosium contaminants (^{156,160}Tb, ^{155,157,159}Dy) has been evaluated too.

1 Introduction

For long time in nuclear medicine, radionuclides have been categorised as diagnostic or therapeutic according to their physical properties and consequently they have been used for labelling different radiopharmaceuticals. However, the use of the same radiopharmaceutical for both diagnosis and therapy, namely for "theranostic", provide some relevant advantages. In fact, by using the same targeting agent, the distribution of the radioactivity within the human body that is measured with a PET (Positron Emission Tomography) or a SPECT (Single Photon Emission Computed Tomography) scanner, undergoes only minor variations in the therapeutic phase. This leads to a more accurate dosimetry in the latter phase [1]. Moreover, if two different radioisotopes of the same element are used as a theranostic couple, the labelled-radiopharmaceuticals appear to be chemically indistinguishable by the biological mechanism in which they are involved and the radioactivity distribution remains unchanged.

The growing interest of the scientific community on the terbium family is justified by the fact that it presents four medically relevant radioisotopes, namely ^{149}Tb, ^{152}Tb, ^{155}Tb and ^{161}Tb, that could be employed either in diagnostic and therapy, and thus becoming a powerful theranostic tool in nuclear medicine [2].

^{149}Tb (I_{α}=16.7%, I_{ec,β^+}=83.3%, $T_{1/2}$= 4.118 h [3]) has been proposed for targeted alpha therapy and preclinical studies have been performed [4, 5]. Alpha particles have the advantages of being short ranged and having high LET (Linear Energy Transfer), in the case of ^{149}Tb those values are 25 μm and 140 keV/μm, respectively [6]. The short range of alpha particles permits to bind cancer cells with low harm to healthy tissues, while high LET particles induce a high number of double-strand breaks in DNA that the cell is not able to repair in an efficient way leading to the death of the cell. These features are particularly useful for the treatment of small metastasis [7]. The full theranostic potential of this isotope has been proved by showing the feasibility of alpha-PET preclinical studies due to competing β^+-decay [8].

^{152}Tb (I_{ec,β^+} = 100%, $T_{1/2}$= 17.5 h [3]) has suitable physical characteristics for PET imaging. It has been used to label DOTANOC [9] for preclnical PET studies in small animals, and for the first human PET/CT scan with ^{152}Tb labelled PSMA-617 [10]. The

Michele Colucci and Stefano Carminati have contributed equally.

[a] e-mail: michele.colucci@unimi.it (corresponding author)
[b] e-mail: stefano.carminati3@studenti.unimi.it
[c] e-mail: haddad@subatech.in2p3.fr
[d] e-mail: nigron@subatech.in2p3.fr
[e] e-mail: flavia.groppi@mi.infn.it
[f] e-mail: simone.manenti@unimi.it (corresponding author)

Published online: 26 October 2022

image quality is not high as the one that can be obtained using conventional ^{68}Ga-PSMA-11, but it has been highlighted its potential use in pre-treatment dosimetry of radiolanthanides therapy.

^{155}Tb (I_{ec}= 100%, $T_{1/2}$= 5.32 d [3]) emits γ-rays suitable for SPECT studies and no β^+/β^- are emitted [11]. It has been demonstrated at preclinical level that this isotope produces good quality SPECT images and it may represent a good alternative to ^{111}In in the diagnostic phase of the therapy with radiolanthanides [1].

^{161}Tb (I_{β^-}= 100%, $T_{1/2}$= 6.89 d [3]) has decay properties (half-life, beta energy and chemical properties) similar to the well-established ^{177}Lu (I_{β}^{-}= 100%, $T_{1/2}$=6.6443 d) [12], but it also emits low energy Auger and conversion electrons ($\sim$ 2.24 e^-/decay) [13] that have a high therapeutic potential due to the high LET (4-26 keV/μm) and the short range (<1μm) [14]. Electrons with these characteristics release the whole energy within a single cancer cell or a small group of them [15]. Moreover, low energy γ-rays are emitted (E_γ= 74.56711 keV I_γ= 10.2%) that make it possible to perform SPECT acquisitions. The latter feature enabled Baum et al. [16] to demonstrate the feasibility of human therapeutic treatment with ^{161}Tb.

The major challenge for the diffusion of the above-mentioned terbium radioisotopes in the clinical practice is related to the difficulty in obtaining them in high amount ($\sim$ GBq) and with high radionuclidic purity. Comprehensive reviews of the production routes of terbium isotopes have been drawn up by Qaim et al. [17] and by Naskar et al. [2]. ISOL technique exploits spallation reactions induced by very energetic protons (e.g. E_p= 1.4 GeV at CERN-ISOLDE [18]) coupled with online separation of isotopes. This technique has been used to obtain enough activity of terbium to perform pre-clinical studies [19]. The drawback of this technique is the very limited number of dedicated facilities [2] like CERN MEDICIS (Medical Isotopes Colleced from ISOLDE) [20] in Switzerland. Only ^{161}Tb can be produced with (n,γ) reaction on highly-enriched ^{160}Gd targets [12]. To this day the studied production routes with light charged particles (p,d, α) are not able to provide Tb quantities that fulfil the clinical requirements. The need for further studies on innovative production routes has been highlighted in the literature [1].

This work aims to determine the cross sections of nuclear reactions induced by deuterons on ^{nat}Dy in the 12.5–32-5 MeV energetic range of the incident beam, with particular attention to the production of ^{155,161}Tb and their long lived contaminants. At present, only one study has been done by Tàrkànyi et al. [21] investigating the same reactions up to 50 MeV. The goal of the present experiment is to verify the nuclear data that are present in the literature and to provide more dense dataset to better estimate the Thick Target Yield (TTY).

2 Materials and methods

The excitation functions were experimetally determined by using the stacked-foils technique. Four different stacks have been prepared, each of them containing four ^{nat}Dy targets. The structure of the stack consists of an alternation between Dy-Al and Ti-Al couples, where the aluminium foils are used as catchers and monitors and titanium foils as monitors. Moreover, three or four aluminium foils have been used as degrader before each Dy foil to reach the desired incident energy on the following Dy target.

The dysprosium (purity 99%, nominal thickness 25μm and 50μm), aluminium (purity 99.999%, nominal thickness 16μm, 25 and 50μm), and titanium (purity 99.9%, nominal thickness 20μm) foils were purchased from Goodfellow Corporation (Hamburg, Germany). For each of them the uniformity was verified using an analogical specimeter and the mass-thickness was determined by measuring the mass and the area: Ti, 8.09 mg$\cdot$ cm^{-2}; Al, in the range between 4.47−43.18 mg$\cdot$ cm^{-2}. The dysprosium targets were measured individually due to the lower uniformity on the whole foil, obtaining mass-thicknesses in the range between 19.3−44.7 mg$\cdot$ cm^{-2}. The uncertainty on these values is lower that 1%. Then squares were cut with $2.5 \times 2.5 cm^2$ dimensions in order to be placed in a metal sample holder for the irradiation.

2.1 Irradiation setup

The irradiations were carried out by accelerating deuterons with the high intensity cyclotron (IBA-C70XP, K=70) of GIP ARRONAX research centre in Saint-Herblain (FR) [22].

The stacks were positioned in air at a distance of about 7 cm from the end of the beam line, which is closed by a 50 μm Kapton window. The shape and the position of the beam were checked by irradiating an Al_2O_3 scintillating foil.

Four irradiations with different incident beam energies were performed on a total of 16 natural dysprosium targets, covering the energy interval between 12.5 and 32 MeV, with a constant current of about 150 nA for a duration of 1 h. The initial energies have been selected by ensuring that the energy range of two consecutive irradiation sessions share at least one point as reported in Table 1. During the irradiation, the beam current stability was monitored using a beam dump combined with a current integrator. The integrated charge and the beam energy were verified by comparing the experimental cross sections of the monitor reactions ^{nat}Ti(d,x)^{48}V and ^{nat}Al(d,x)^{24}Na with the IAEA recommended ones [23]. The results are reported in Figs. 1 and 2. The agreement between the experimental data and the recommended curves is high. In particular, there is low or no discrepancy between various irradiation sessions, increasing the reliability of the obtained results.

Table 1 Medium energy of the deuterons in each dysprosium foil

	E_1 (MeV)	$E_2(MeV)$	E_3 (MeV)	E_4 (MeV)
1^{st} Stack	31.8 ± 0.7	30.2 ± 0.8	28.7 ± 0.8	27.1 ± 0.8
2^{nd} Stack	28.6 ± 0.6	27.1 ± 0.6	25.6 ± 0.7	24.0 ± 0.7
3^{rd} Stack	24.8 ± 0.5	23.0 ± 0.6	21.1 ± 0.6	19.0 ± 0.6
4^{th} Stack	19.8 ± 0.5	17.6 ± 0.5	15.3 ± 0.5	12.8 ± 0.5

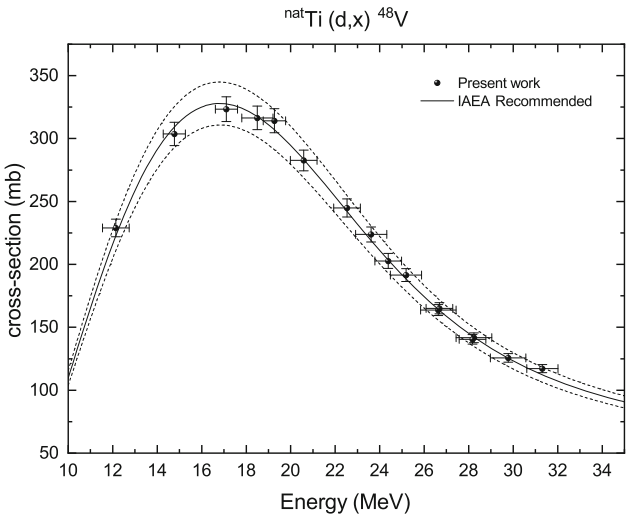

Fig. 1 Cross section of the monitor reaction ^{nat}Ti(d,x)^{48}V. The experimental results are compared with the IAEA recommended curve [23], dashed line corresponds to the IAEA uncertainty band. All the points are contained within the error band and no discrepancies are present between the points obtained in different irradiation sessions

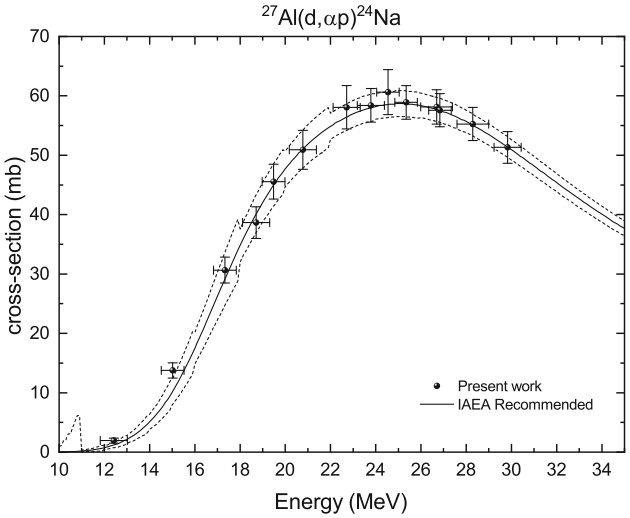

Fig. 2 Cross section of the monitor reaction ^{nat}Al(d,x)^{24}Na. The experimental results are compared with the IAEA recommended curve [23], dashed line corresponds to the IAEA uncertainty band. There is major agreement between the experimental data and the recommended curve

2.2 Measurements

The activity measurements of the targets were performed without any chemical processing at the LASA Laboratory (INFN and Physics Department of University of Milano, Segrate, MI) employing high purity germanium (HPGe) detectors. Each detector was calibrated in energy and efficiency with certified ^{152}Eu and ^{133}Ba sources (CercaLEA, France and Amersham, UK). ^{133}Ba point source has been used in order to determine the efficiency at low energy exploiting the 53.162 keV (I_γ=2.14%), 80.99 keV (I_γ=32.9%) and 160.61 keV (I_γ=0.638%) gamma-ray lines.

The measurements started two days after the bombardments and continued for about 3 – 4 months, in order to collect a large set of data to reduce the uncertainties on the quantities of interest. The duration of the measurements ranged between 30 min – 2 d. The source-detector distance was chosen in order to obtain a dead time of the detectors always lower than 3%.

The radionuclides for which the cross sections were measured are shown in Table 2 with their nuclear data [3], contributing reactions and the related threshold energies.

Table 2 Nuclear decay data and contributing reactions [3]. The most intense γ-rays are reported. The ones used to determine the cross sections are bolded

Nuclide	Half-life	$E_\gamma(keV)$	$I_\gamma(\%)$	Contributing reactions	$E_{thr}(MeV)$
^{155}Tb	5.32 *d*	86.545	32.03	$^{156}Dy(d,2pn)$	8.906
ec (100%)		**105.305**	**25.1**	$^{158}Dy(d,2p3n)$	25.00
		180.103	**7.45**	$^{160}Dy(d,2p5n)$	38.58
^{156}Tb	5.35 *d*	88.9667	17.67	$^{156}Dy(d,2p)$	1.89
ec, β^+ (100%)		**199.2132**	**40.92**	$^{158}Dy(d,\alpha)$	0
		262.579	5.766	$^{158}Dy(d,2p2n)$	18.02
		356.426	13.6	$^{160}Dy(d,2p4n)$	31.60
		422.38	7.9	$^{161}Dy(d,2p5n)$	39.99
		534.318	**66.59**	$^{156m_2}Tb \rightarrow ^{156}Tb$	
		1065.15	10.77	$^{156m_1}Tb \rightarrow ^{156}Tb$	
		1154.19	10.37		
		1159.04	7.34		
		1222.36	31		
^{160}Tb	72.3 *d*	86.7882	13.8	$^{162}Dy(d,\alpha)$	0
β^- (100%)		197.0352	5.18	$^{160}Dy(d,2p)$	1.51
		298.58	**26.1**	$^{161}Dy(d,2pn)$	9.90
		879.383	**30.1**	$^{162}Dy(d,2p2n)$	18.11
		962.317	9.81	$^{163}Dy(d,2p3n)$	24.42
		966.171	25.1	$^{164}Dy(d,2p4n)$	32.06
		1177.962	14.9		
		1271.88	7.44		
^{161}Tb	6.88 *d*	25.6515	23.2	$^{163}Dy(d,\alpha)$	0
β^- (100%)		48.91562	17	$^{161}Dy(d,2p)$	2.17
		74.56711	**10.2**	$^{162}Dy(d,2pn)$	10.37
				$^{163}Dy(d,2p2n)$	16.69
				$^{164}Dy(d,2p3n)$	24.33
^{155}Dy	9.9 *h*	**226.918**	**68.4**	$^{156}Dy(d,p2n)$	11.79
β^+ (100%)		1155.47	2.08	$^{158}Dy(d,p4n)$	27.92
				$^{155}Ho \rightarrow ^{155}Dy$	
^{157}Dy	8.14 *h*	**326.16**	**92**	$^{158}Dy(d,p2n)$	11.41
β^+ (100%)				$^{160}Dy(d,p4n)$	25.00
				$^{161}Dy(d,p5n)$	33.39
				$^{157}Ho \rightarrow ^{157}Dy$	
^{159}Dy	144.4 *d*	**58**	**2.22**	$^{158}Dy(d,p)$	0
ec (100%)				$^{160}Dy(d,p2n)$	8.96
				$^{161}Dy(d,p3n)$	17.35
				$^{162}Dy(d,p4n)$	25.56
				$^{163}Dy(d,p5n)$	31.87
				$^{159}Ho \rightarrow ^{159}Dy$	

3 Results

The determination of the cross section has been done by measuring the activity produced on each thin foil in a highly reproducible geometry: the targets have been positioned on top of a spacer with the beam entrance side facing the detector. The cross section σ(E) (mb) is computed through Eq. (1) [24]:

$$\sigma(E) = \frac{NCounts_\gamma}{\varepsilon_\gamma \cdot I_\gamma \cdot LT \cdot Q} \cdot \frac{M \cdot Z \cdot e}{\lambda \cdot N_A \cdot \rho dx} \cdot D(RT) \cdot G(t_{irr}) \cdot e^{\lambda \cdot \Delta t} \quad (1)$$

where $NCounts_\gamma$ is the net photo-peak counts at the energy E_γ, E (MeV) is the mean energy of the deuteron beam within the thin foil, ε_γ is the efficiency of the HPGe at the energy E_γ, I_γ denotes the absolute abundance of γ, LT is the Live counting Time (s), RT is the Real counting Time and is given by the sum of LT and the dead time DT, t_{irr} (s) is the duration of the irradiation, Δt is the time between the End-Of-Bombardment and the beginning of the measurement, therefore the factor $e^{\lambda \cdot \Delta t}$ corrects for the

Table 3 Experimental cross section of the reactions ^{nat}Dy(d,x)^{1yy}Tb

$E_d(MeV)$	ΔE (MeV)	Cross section $\sigma \pm \Delta\sigma$ (mb)			
		^{155}Tb (cum)	^{156}Tb	^{160}Tb	^{161}Tb
31.8	0.7	0.63 ± 0.03	0.48 ± 0.02	4.1 ± 0.2	2.69 ± 0.10
30.2	0.8	0.63 ± 0.04	0.306 ± 0.012	3.8 ± 0.2	2.66 ± 0.12
28.7	0.8	0.61 ± 0.04	0.190 ± 0.008	3.5 ± 0.2	2.43 ± 0.12
28.6	0.6	0.62 ± 0.04	0.170 ± 0.010	3.4 ± 0.2	2.44 ± 0.11
27.1	0.6	0.56 ± 0.03	0.108 ± 0.006	2.99 ± 0.18	2.07 ± 0.12
27.1	0.8	0.54 ± 0.03	0.106 ± 0.006	2.97 ± 0.17	2.12 ± 0.12
25.6	0.7	0.46 ± 0.03	0.057 ± 0.006	2.51 ± 0.15	1.96 ± 0.10
24.8	0.5	0.45 ± 0.02	0.061 ± 0.002	2.45 ± 0.15	1.96 ± 0.07
24.0	0.7	0.38 ± 0.02	0.036 ± 0.004	2.25 ± 0.014	1.86 ± 0.09
23.0	0.6	0.31 ± 0.02	0.0273 ± 0.0016	2.10 ± 0.13	1.86 ± 0.07
21.1	0.6	0.20 ± 0.01	0.0179 ± 0.0012	1.85 ± 0.11	1.77 ± 0.07
19.8	0.5	0.12 ± 0.01	0.0115 ± 0.0007	1.62 ± 0.09	1.62 ± 0.07
19.0	0.6	0.061 ± 0.002	0.0139 ± 0.0007	1.46 ± 0.09	1.38 ± 0.07
17.6	0.5	0.033 ± 0.002	0.0099 ± 0.0006	1.31 ± 0.07	1.17 ± 0.06
15.3	0.5	0.021 ± 0.003	0.0066 ± 0.0004	0.82 ± 0.05	0.76 ± 0.03
12.8	0.5	0.007 ± 0.002	0.0113 ± 0.0009	0.52 ± 0.03	0.51 ± 0.02

decay during the time Δt, Q is the integrated charge of the deuteron beam (C), Z·e is the deuteron charge (C), M is the atomic mass (g· mol^{-1}), N_A is the Avogadro number (atoms· mol^{-1}) and ρ dx is the experimental mass-thickness (g· cm^{-2}) of the foil. Two correction factors are used, namely the decay factor D(RT) that corrects for the decay during RT, and the growing factor G(t_{irr}) that takes into account the decay during t_{irr}. Those two dimensionless factors are defined as:

$$D(RT) = \frac{\lambda \cdot RT}{1 - e^{-\lambda \cdot RT}} \tag{2}$$

and

$$G(t_{irr}) = \frac{\lambda \cdot t_{irr}}{1 - e^{-\lambda \cdot t_{irr}}}. \tag{3}$$

The factors that contribute to the uncertainty budget are reported by Manenti et al. [25]. In particular, the uncertainty on the $NCounts_\gamma$ has been kept lower than 7%, with a overall uncertainty of (3 – 10)% depending on the radionuclide.

The experimental excitation functions are reported in Figs. 3, 4, 5, 6, 7, 8 and 9, compared with a previous nuclear dataset from Tàrkànyi et al. [21]. The numerical results are listed in Tables 3 and 4. Theoretical simulations with default options were performed with EMPIRE−3.2.3 [26] and TALYS 1.96 [27] computer codes. Despite the good simulation results for the other reactions, the former code does not describe properly the experimental results of ^{nat}Dy(d,x)^{1yy}Tb reactions, and generally it overestimates the experimental results. It is possible that the default options are not appropriate for the modelling of the nuclear properties of terbium nuclei. Nevertheless, they are reported in Figs. 3, 4, 5 and 6 for the sake of completeness.

3.1 ^{nat}Dy(d,x)^{155}Tb(cum)

The cross section reported in Fig. 3 refers to the cumulated production of ^{155}Tb by means of the direct production via the ^{nat}Dy(d,x)^{155}Tb and of the contribution of the decay of ^{155}Dy. To measure the cumulative cross section a time of about 10 half-lives of ^{155}Dy has been waited.

Two γ emission has been used to determine its activity on each foil: E_γ=105.305 keV (I_γ=25.1%) and E_γ=180.103 keV (I_γ=7.45%). The most intense γ-ray emission at E_γ=86.545 keV (I_γ=32.03%) could not be used due to the superposition with γ-ray emission at E_γ=86.7882 keV (I_γ=13.8%) of ^{160}Tb ($T_{1/2}$=72.3 d).

This is the only reaction with a terbium radioisotope as product that the EMPIRE 3.2.3 code with default options is able to describe properly. This is probably due to the fact that the main contribution to the production of ^{155}Tb is given by the decay of ^{155}Dy as it can be deducted from the comparison between the cross sections (see Table 3 and 4).

The accordance with the other experimental results and with TALYS 1.96 calculations is low. However, as explained in Sect. 2.1, due to the experimental procedure that has been followed, the confidence in the results is high. Moreover, there is accordance between the activity measured with the two gamma-rays selected and low uncertainty is obtained by performing different repetitions of the measurements.

Table 4 Experimental cross section of the reactions ^{nat}Dy(d,x)^{1yy}Dy

$E_d(MeV)$	$\Delta E\ (MeV)$	Cross section $\sigma \pm \Delta\sigma\ (mb)$		
		^{155}Dy (cum)	^{157}Dy (cum)	^{159}Dy (cum)
31.8	0.7	0.66 ± 0.05	1.20 ± 0.12	144 ± 6
30.2	0.8	0.60 ± 0.05	1.29 ± 0.09	115 ± 5
28.7	0.8	0.60 ± 0.06	1.43 ± 0.11	99 ± 5
28.6	0.6	0.58 ± 0.03	1.38 ± 0.06	101 ± 5
27.1	0.6	0.51 ± 0.03	1.20 ± 0.05	69 ± 3
27.1	0.8	0.52 ± 0.04	1.20 ± 0.10	70 ± 5
25.6	0.7	0.44 ± 0.03	1.05 ± 0.07	47 ± 2
24.8	0.5	0.44 ± 0.02	1.02 ± 0.05	38.3 ± 1.6
24.0	0.7	0.38 ± 0.02	0.96 ± 0.05	31.1 ± 1.4
23.0	0.6	0.317 ± 0.015	0.82 ± 0.04	26.9 ± 1.2
21.1	0.6	0.164 ± 0.007	0.61 ± 0.03	19.9 ± 0.9
19.8	0.5	0.113 ± 0.005	0.48 ± 0.02	18.5 ± 0.8
19.0	0.6	0.078 ± 0.004	0.349 ± 0.016	15.3 ± 0.7
17.6	0.5	0.020 ± 0.001	0.213 ± 0.010	14.1 ± 0.5
15.3	0.5		0.203 ± 0.010	13.3 ± 0.6
12.8	0.5		0.236 ± 0.012	10.8 ± 0.4

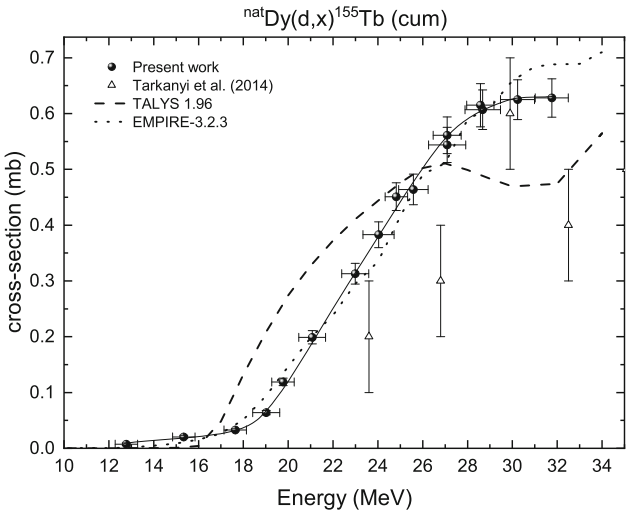

Fig. 3 Cumulative cross section of the reaction ^{nat}Dy(d,x)^{155}Tb. The experimental results are compared with the data of Tàrkànyi et al. [21] and with the theoretical simulations. An eye-guideline (solid line) has been added to easily visualise the data. Low accordance is detected between the experimental data, the previous dataset and the TALYS 1.96 code

3.2 ^{nat}Dy(d,x)^{156}Tb

^{156}Tb ($T_{1/2}$=5.35 d) is the main contaminant in the production of ^{155}Tb due to its similar decay time. The activity was determined by using the 199.213 keV (I_γ=40.9%) and the 534.318 keV (I_γ=66.59%) γ-ray emissions. The results are shown in Fig. 4. There is low accordance with the previous experimental data and with TALYS−1.96 calculations. EMPIRE 3.2.3 computer code overestimates the experimental data.

3.3 ^{nat}Dy(d,x)^{160}Tb

Due to the long decay time of ^{160}Tb, it is generally considered to be the main contaminant of the therapeutic ^{161}Tb [28]. The most intense γ-ray emissions of ^{160}Tb are the same of the co-produced $^{160(m+g)}$Ho ($T_{1/2}(^{160m}$Ho)=5.02 h), thus to determine the activity of ^{160}Tb a whole week from the end of the irradiation was waited to make sure that $^{160(m+g)}$Ho completely decayed. The 298.58 keV (I_γ=26.1%) and the 879.383 keV (I_γ=30.1%) γ-ray emissions has been used to calculate the activity. The cross section is presented in Fig. 5. It is in agreement with the results of Tàrkànyi et al. [21], but the simulation codes does not reproduce correctly the experimental data. In particular EMPIRE 3.2.3 code overestimate the experimental results and cannot be seen in the graph for energy higher than 13 MeV.

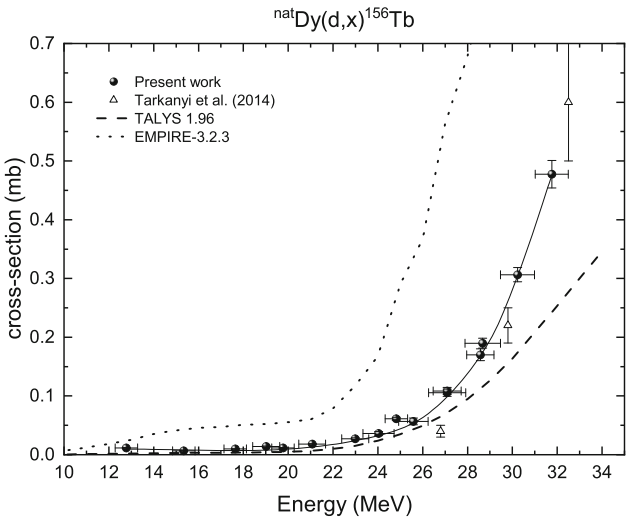

Fig. 4 Cross section of the reaction ^{nat}Dy(d,x)^{156}Tb. The experimental results are compared with the data of Tàrkànyi et al. [21] and with the theoretical simulations. An eye-guideline (solid line) has been added to easily visualise the data

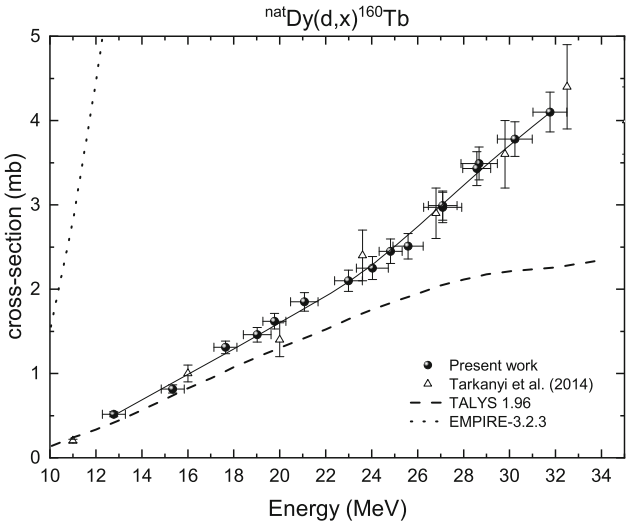

Fig. 5 Cross section of the reaction ^{nat}Dy(d,x)^{160}Tb. The experimental results are compared with the data of Tàrkànyi et al. [21] and with the theoretical simulations. An eye-guideline (solid line) has been added to easily visualise the data. The simulation performed with EMPIRE 3.2.3 exceeds the scale used to properly visualise the excitation function

3.4 ^{nat}Dy(d,x)^{161}Tb

The only γ-ray emission associated with the decay of ^{161}Tb that can be efficiently detected by a p-type HPGe detector is the one at 74.56711 keV (I_γ=10.2%). The experimental results are reported in Fig. 6. They are compatible with the existing dataset [21], while the agreement with the TALYS 1.96 simulation is low. In the inset of Fig. 6, there is the same graph with a different scale that permits to appreciate the large overestimation that the EMPIRE 3.2.3 code introduces.

3.5 ^{nat}Dy(d,x)^{155}Dy (cum)

The cross section of the reaction ^{nat}Dy(d,x) ^{155}Dy, cumulated with the contribution of the decay of the co-produced ^{155}Ho, is reported in Fig. 7. ^{155}Dy decays *ec*, β^+ (100%) with a half-life of 9.9 h. The γ-ray used to evaluate the activity has energy E_γ=226.928 keV (I_γ=65.4%). The results are compatible with the cross section measured in the previous dataset [21], taking into accounting the error bars, and with the calculation of EMPIRE−3.2.3. The accordance of the simulation performed with TALYS 1.96 is low.

Moiseeva et al. [29] demonstrated that ^{155}Dy can be employed as a generator for ^{155}Tb. However, this production pathway (^{nat}Dy+d) gives rise to the co-production of other radioisotopes of Dy as ^{157}Dy that decays with a similar half-life (8.14 h) producing ^{157}Tb, and this would result in a low specific activity of the eluted solution.

3.6 ^{nat}Dy(d,x)^{157}Dy (cum)

The decay of ^{157}Dy comes with an intense γ-ray emission at $E_\gamma = 326.16$ keV (I_γ=92 %) that has been used to calculate the cross section of the reaction ^{nat}Dy(d,x)^{157}Dy (cum). It is not possible to separate the contribute of the direct reaction from the indirect production via the decay of ^{157}Ho due to the short half-life of the latter ($T_{1/2}$=12.6 min). The excitation function is reported in

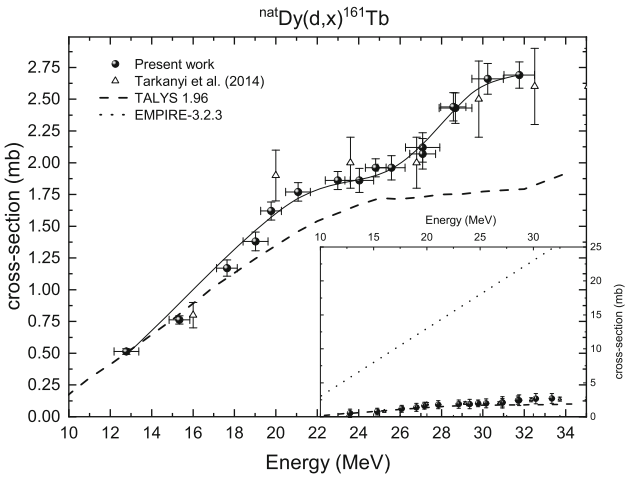

Fig. 6 Cross section of the reaction ^{nat}Dy(d,x)^{161}Tb. The experimental results are compared with the data of Tàrkànyi et al. [21] and with the theoretical simulations. An eye-guideline (solid line) has been added to easily visualise the data. **Inset**: a larger scale visualisation of the graph that permits to see the result of the EMPIRE 3.2.3 code simulation with default options

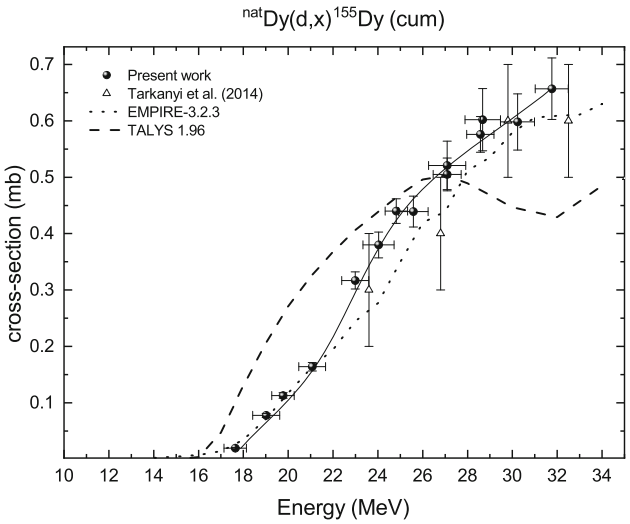

Fig. 7 Cumulative cross section of the reaction ^{nat}Dy(d,x)^{155}Dy. The experimental results are compared with the data of Tàrkànyi et al. [21] and with the theoretical simulations. An eye-guideline (solid line) has been added to easily visualise the data

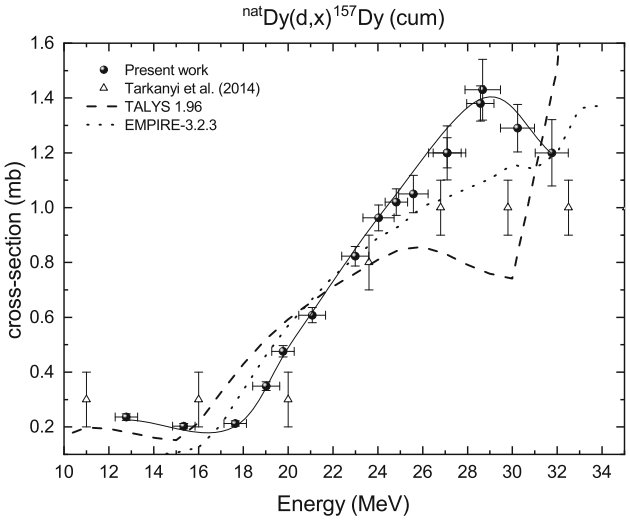

Fig. 8 Cumulative cross section of the reaction ^{nat}Dy(d,x)^{157}Dy (cum). The experimental results are compared with the data of Tàrkànyi et al. [21] and with the theoretical simulations. An eye-guideline (solid line) has been added to easily visualise the data. The agreement of the previous dataset and the simulation with the experimental data at energy higher than 24 MeV is low

Fig. 8. The compatibility with the other experimental data and with the simulations is high at low energies, while at energies higher than 24 MeV the results of the present experiment show a different behaviour. The confidence in the results of the present work is high because the data in the energy range down to 24 MeV result from the overlapping of three different irradiation sessions (see Sect. 2.1) and low discrepancies are present between them.

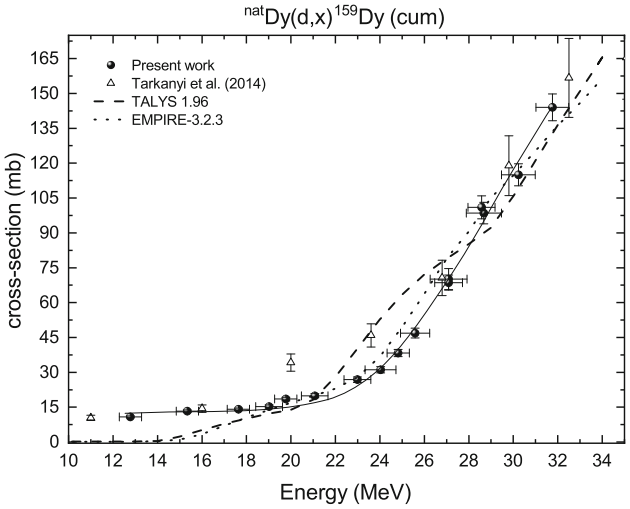

Fig. 9 Cumulative cross section of the reaction ^{nat}.Dy(d,x)^{159}Dy The experimental results are compared with the data of Tàrkànyi et al. [21] and with the theoretical simulations. An eye-guideline (solid line) has been added to easily visualise the data

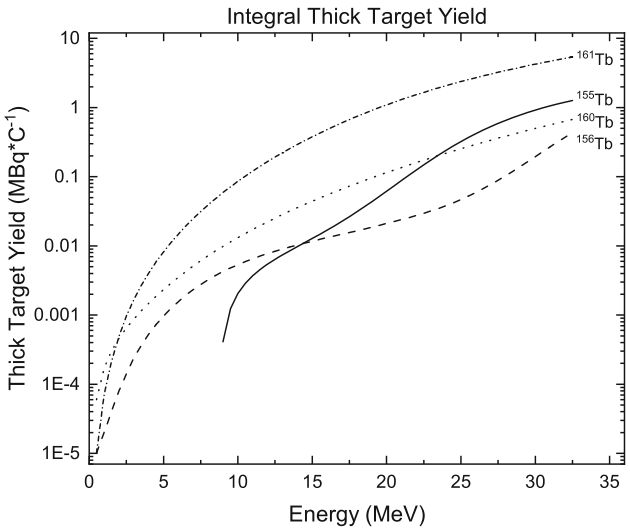

Fig. 10 Thick Target Yield in the total absorption condition for the production of ^{155,156,160,161}Tb

3.7 ^{nat}Dy(d,x)^{159}Dy (cum)

^{159}Dy is a long lived radioisotope of dysprosium ($T_{1/2}$=144.4 d) and decays via electron capture. The most intense γ-ray is emitted at the energy of 58 keV and has an intensity of 2.22 %. The experimental data are reported in Fig. 9. The accordance with the experimental results from Tàrkànyi et al. [21] and with the theorical calculations performed with both TALYS 1.96 and EMPIRE−3.2.3, is good. However, it should be noticed that experimental data present a low energy plateau that is not described by the codes. As seen in Table 2, different reactions with low or no threshold are possible and the description of these production routes may not be well reproduced by the theoretical calculations.

3.8 Thick Target Yield

The TTY, Y(E,ΔE), has been calculated as reported in Eq. (4) [30]:

$$Y(E, \Delta E) = \frac{N_A \cdot \lambda}{M \cdot e} \int_{E-\Delta E}^{E} \sigma(E') \frac{dE'}{S(E')}, \tag{4}$$

where E' is the integration variable, E is the incident energy, ΔE is the energy loss within the thick target, S(E) is the mass stopping power of the deuteron beam through the target at the energy E (S(E)=dE/d(ρx)), while the other terms have been defined in Eq. (1). In the case of total absorption, the lower limit of integration is zero for reaction without threshold, otherwise it is equal to E_{thr}.

The calculated TTYs in the condition of total absorption are reported in Fig. 10 in the case of terbium radioisotopes, and in Fig. 11 in the case of the other contaminants. The calculation has been extended in energy down to zero, with exception of ^{155}Tb, ^{155}Dy and ^{157}Dy for which a threshold energy is present.

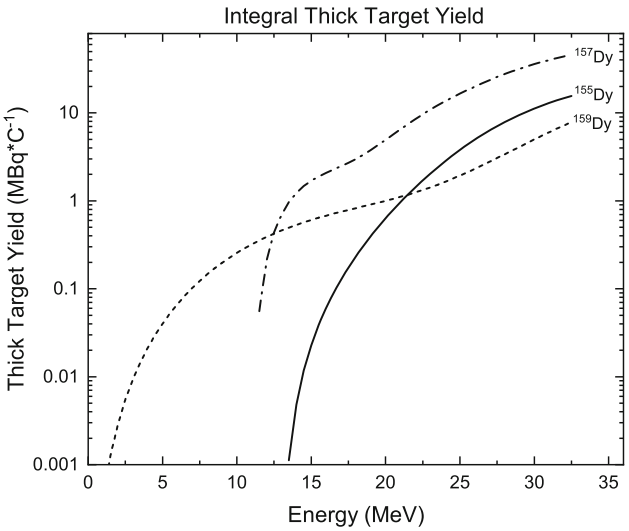

Fig. 11 Thick Target Yield in the total absorption condition for the production of ^{155,157,159}Dy

In condition of total absorption the TTY of ^{161}Tb is of 5.4 MBq·C^{-1} at 32 MeV or, equivalently of $1.94 \cdot 10^{-2}$ MBq in 1 h of irradiation at 1 μA. This rate is too low compared to the activities that are required for pre-clinical and clinical applications (∼GBq). The same is true for ^{155}Tb, whose TTY is of 1.3 MBq·C^{-1} ($4.68 \cdot 10^{-3}$ MBq/μA·h) at 32 MeV in condition of total absorption.

The co-production of ^{160}Tb and of ^{156}Tb is unavoidable with a natural dysprosium target and it is not possible to separate them chemically. Moreover, it is reasonable to state that the cross section of the production of ^{157}Tb ($T_{1/2}$=71 y) and of ^{158}Tb ($T_{1/2}$=180 y) is not negligible and their presence reduces the radionuclidic purity and the specific activity [31] of the product.

4 Conclusion

The possibility to produce two of the four theranostic relevant radioisotopes of terbium via deuterons irradiation of natural dysprosium targets has been discussed in this paper. The cross section of the nuclear reactions ^{nat}Dy(d,x)^{155,161}Tb in the energetic range of 12.5 – 32 MeV has been measured, and the coproduction of terbium and dysprosium contaminants (^{156,160}Tb and ^{155,157,159}Dy) has been evaluated too.

The experimental excitation functions have been compared to a previous dataset by Tàrkànyi et al. [21] resulting in a general agreement with some exceptions for ^{155}Tb and ^{157}Dy. The accordance with the theoretical simulation performed with EMPIRE 3.2.3 and with TALYS 1.96 using default options is for the most part insufficient.

The TTY, in condition of total absorption and with the entrance beam energy of 32 MeV, is generally low: it has been estimated to be 5.4 MBq·C^{-1} in the case of ^{161}Tb and 1.3 MBq·C^{-1} for ^{155}Tb. The order of magnitude of the TTY of co-production of terbium contaminants is comparable to the former and this make even more challenging the use of this production route.

The indirect production route of ^{155}Tb via the decay of ^{155}Dy has been evaluated too. However the TTY of the production of ^{157}Dy is higher that the one of the radionuclide of interest. It should be considered the possibility to enrich the target in ^{156}Dy. Even if it is impossible to avoid the co-production of ^{157}Dy, further studies on enriched targets could highlight energy ranges in which is possible to obtain a ^{155}Dy-^{155}Tb generator with high specific activity of the final product.

Ultimately, this work achieved the goal to provide new and denser nuclear data that will allow more precise theoretical calculations on terbium and dysprosium nuclei.

Acknowledgements This work was funded in the framework of the research project REMIX by INFN (Italian National Institute of Nuclear Physics, CSN5). The ARRONAX cyclotron is a project promoted by the Regional Council of Pays de la Loire financed by local authorities, the French government, and the European Union. This work has been, in part, supported by a grant from the French National Agency for Research called "Investissements d'Avenir", Equipex Arronax-Plus No. ANR-11-EQPX-0004 and Labex No. ANR- 11-LABX-0018-01. It has been also supported partly through a funding from the European Union's Horizon 2020 research and innovation programme under grant agreement No 101008571 (PRISMAP).

Funding Open access funding provided by Università degli Studi di Milano within the CRUI-CARE Agreement.

Data Availibility Statement No Data associated in the manuscript.

References

1. C. Müller, K.A. Domnanich, C.A. Umbricht, N.P. van der Meulen, Scandium and terbium radionuclides for radiotheranostics: current state of development towards clinical application. Br. J. Radiol. **91**(1091), 20180074 (2018). https://doi.org/10.1259/bjr.20180074. (**PMID: 29658792**)
2. N. Naskar, S. Lahiri, Theranostic terbium radioisotopes: challenges in production for clinical application. Front.Med. (2021). https://doi.org/10.3389/fmed.2021.675014
3. R.B. Firestone, S.Y.F. Chu, C.M. Baglin, 8th edition of the Table of Isotopes: 1998 Update. In: APS Division of Nuclear Physics Meeting Abstracts. APS Meeting Abstracts, p. 11 (1997)
4. G.J. Beyer, M. Miederer, S. Vranješ-Durić, J.J. Čomor, G. Künzi, O. Hartley, R. Senekowitsch-Schmidtke, D. Soloviev, F. Buchegger, Targeted alpha therapy in vivo: direct evidence for single cancer cell kill using ^{149} Tb -rituximab. Eur. J. Nucl. Med. Mol. Imaging **31**, 547–554 (2004). https://doi.org/10.1007/s00259-003-1413-9
5. C. Müller, J. Reber, S. Haller, H. Dorrer, U. Köster, K. Johnston, K. Zhernosekov, A. Türler, R. Schibli, Folate receptor targeted alpha-therapy using terbium-149. Pharmaceuticals **7**, 353–365 (2014). https://doi.org/10.3390/ph7030353
6. S.K. Imam, Advancements in cancer therapy with alpha-emitters: a review. Int J Rad Oncol Phy. **51**(1), 271–278 (2001). https://doi.org/10.1016/s0360-3016(01)01585-1
7. M. Sollini, K. Marzo, A. Chiti, M. Kirienko, The five "w"s and "how" of targeted alpha therapy: why? who? what? where? when? and how? Rendiconti Lincei **31**, 231–247 (2020). https://doi.org/10.1007/s12210-020-00900-2
8. C. Müller, C. Vermeulen, U. Köster, K. Johnston, A. Türler, R. Schibli, N.P. van der Meulen, Alpha-PET with terbium-149: evidence and perspectives for Radiotheragnostics. EJNMMI Radiopharm. Chem. (2016). https://doi.org/10.1186/s41181-016-0008-2
9. C. Müller, C. Vermeulen, K. Johnston, U. Köster, R. Schmid, A. Türler, N.P. van der Meulen, Preclinical in vivo application of ^{152} Tb -DOTANOC: a Radiolanthanide for PET imaging. EJNMMI Research (2016). https://doi.org/10.1186/s13550-016-0189-4
10. C. Müller, A. Singh, C.A. Umbricht, H.R. Kulkarni, K. Johnston, M. Benešová, S. Senftleben, D. Müller, C. Vermeulen, R. Schibli, U. Köster, N.P. van der Meulen, R.P. Baum, Preclinical investigations and first-in-human application of ^{152} Tb -PSMA-617 for PET/CT imaging of prostate cancer. EJNMMI Research (2019). https://doi.org/10.1186/s13550-019-0538-1
11. C. Müller, E. Fischer, M. Behe, U. Köster, H. Dorrer, J. Reber, S. Haller, S. Cohrs, A. Blanc, J. Grünberg, M. Bunka, K. Zhernosekov, N. van der Meulen, K. Johnston, A. Türler, R. Schibli, Future prospects for SPECT imaging using the Radiolanthanide terbium-155 - production and preclinical evaluation in tumor-bearing mice. Nucl. Med.Biol. **41**, e58-65 (2014). https://doi.org/10.1016/j.nucmedbio.2013.11.002
12. S. Lehenberger, C. Barkhausen, S. Cohrs, E. Fischer, J. Grünberg, A. Hohn, U. Köster, R. Schibli, A. Türler, K. Zhernosekov, The low-energy β - and electron emitter ^{161} Tb as an alternative to ^{177} Lu for targeted radionuclide therapy. Nucl. Med. Biol. **38**, 917–924 (2011). https://doi.org/10.1016/j.nucmedbio.2011.02.007
13. National Nuclear Data Center. https://www.nndc.bnl.gov/
14. F. Buchegger, F. Perillo-Adamer, Y.M. Dupertuis, A.B. Delaloye, Auger radiation targeted into DNA: a therapy perspective. Eur. J. Nucl. Med. Mol. Imaging **33**, 1352–1363 (2006). https://doi.org/10.1007/s00259-006-0187-2
15. D. Filosofov, E. Kurakina, V. Radchenko, Potent candidates for targeted auger therapy: production and radiochemical considerations. Nucl. Med. Biol. **94–95**, 1–19 (2021). https://doi.org/10.1016/j.nucmedbio.2020.12.001
16. R.P. Baum, A. Singh, H.R. Kulkarni, P. Bernhardt, T. Rydén, C. Schuchardt, N. Gracheva, P.V. Grundler, U. Köster, D. Müller, M. Pröhl, J.R. Zeevaart, R. Schibli, N.P. van der Meulen, C. Müller, First-in-human application of terbium-161: a feasibility study using ^{161} Tb -DOTATOC. J. Nucl. Med. **62**, 1391–7 (2021). https://doi.org/10.2967/jnumed.120.258376
17. S.M. Qaim, B. Scholten, B. Neumaier, New developments in the production of theranostic pairs of radionuclides. J. Radioanal. Nucl. Chem. **318**, 1493–1509 (2018). https://doi.org/10.1007/s10967-018-6238-x
18. R. Catherall, W. Andreazza, M. Breitenfeldt, A. Dorsival, G.J. Focker, T.P. Gharsa, T.J. Giles, J.L. Grenard, F. Locci, P. Martins, S. Marzari, J. Schipper, A. Shornikov, T. Stora, The ISOLDE facility. J. Phys. G: Nucl. Particle Phys. **44**, 094002 (2017). https://doi.org/10.1088/1361-6471/aa7eba
19. R.F. Cavaier, F. Haddad, T. Sounalet, T. Stora, I. Zahi, Terbium Radionuclides for Theranostics Applications: A Focus On MEDICIS-PROMED. Physics Procedia **90**, 157–163 (2017). https://doi.org/10.1016/j.phpro.2017.09.053Conference on the Application of Accelerators in Research and Industry, CAARI 2016, 30 October - 4 November 2016, Ft. Worth, TX, USA
20. R.M. dos Santos Augusto, L. Buehler, Z. Lawson, S. Marzari, M. Stachura, T. Stora, CERN-MEDICIS (medical isotopes collected from ISOLDE): A new facility. Applied Sciences (Switzerland) **4**, 265–281 (2014). https://doi.org/10.3390/app4020265
21. F. Tárkányi, F. Ditrói, S. Takács, J. Csikai, A. Hermanne, A.V. Ignatyuk, Activation cross-sections of long lived products of deuteron induced nuclear reactions on dysprosium up to 50 MeV. Appl. Radiat. Isot. **83**, 18–24 (2014). https://doi.org/10.1016/j.apradiso.2013.10.011
22. F. Haddad, L. Ferrer, A. Guertin, T. Carlier, N. Michel, J. Barbet, J.F. Chatal, ARRONAX, a high-energy and high-intensity cyclotron for nuclear medicine. Eur. J. Nucl. Med. Mol. Imaging **35**, 1377–1387 (2008). https://doi.org/10.1007/s00259-008-0802-5
23. A. Hermanne, A.V. Ignatyuk, R. Capote, B.V. Carlson, J.W. Engle, M.A. Kellett, T. Kibédi, G. Kim, F.G. Kondev, M. Hussain, O. Lebeda, A. Luca, Y. Nagai, H. Naik, A.L. Nichols, F.M. Nortier, S.V. Suryanarayana, S. Takács, F.T. Tárkányi, M. Verpelli, Reference cross sections for charged-particle monitor reactions. Nucl. Data Sheets **148**, 338–382 (2018). https://doi.org/10.1016/j.nds.2018.02.009
24. F. Bianchi, C. Marchi, G. Fuad, F. Groppi, F. Haddad, L. Magagnin, S. Manenti, On the production of $^{52\,g}$ Mn by deuteron irradiation on natural chromium and its Radionuclidic purity. Appl. Rad. Isotop. **166**, 109329 (2020). https://doi.org/10.1016/j.apradiso.2020.109329
25. S. Manenti, M. del Carmen Alí, G. Santoro, C. Cotogno, F. Duchemin, U. Haddad, F. Groppi. Holzwarth, Excitation function and yield for the ^{103}Rh(d,2n)^{103}Pd nuclear reaction: optimization of the production of palladium-103. Nucl. Med. Biol. **49**, 30–37 (2017). https://doi.org/10.1016/j.nucmedbio.2017.02.005
26. M. Herman, R. Capote, B.V. Carlson, P. Obložinský, M. Sin, A. Trkov, H. Wienke, V. Zerkin, EMPIRE: Nuclear reaction model code system for data evaluation. Nucl. Data Sheets **108**, 2655 (2007). https://doi.org/10.1016/j.nds.2007.11.003
27. A.J. Koning, D. Rochman, J.-C. Sublet, N. Dzysiuk, M. Fleming, S. van der Marck, TENDL: Complete nuclear data library for innovative nuclear science and technology. Nucl. Data Sheets **155**, 502 (2019). https://doi.org/10.1016/j.nds.2019.01.002
28. F. Szelecsényi, Z. Kovács, K. Nagatsu, M.R. Zhang, K. Suzuki, Investigation of deuteron-induced reactions on ^{nat} Gd up to 30 MeV: possibility of production of medically relevant ^{155} Tb and ^{161} Tb radioisotopes. J. Radioanal. Nucl. Chem. **307**, 1877–1881 (2016). https://doi.org/10.1007/s10967-015-4528-0

29. A.N. Moiseeva, R.A. Aliev, E.B. Furkina, V.I. Novikov, V.N. Unezhev, New method for production of ^{155}Tb via ^{155}Dy by irradiation of ^{nat}Gd by medium energy alpha particles. Nucl. Med. Biol. **106–107**, 52–61 (2022). https://doi.org/10.1016/j.nucmedbio.2021.12.004
30. G. Pupillo, L. Mou, S. Manenti, F. Groppi, J. Esposito, F. Haddad, Nuclear data for light charged particle induced production of emerging medical radionuclides. Radiochim. Acta **110**(6–9), 689–706 (2022). https://doi.org/10.1515/ract-2022-0011
31. J.J.M.D. Goeij, M.L. Bonardi, How do we define the concepts specific activity, radioactive concentration, carrier, carrier-free and no-carrier-added? J. Radioanal. Nucl. Chem. **263**, 13–18 (2005). https://doi.org/10.1007/s10967-005-0004-6